

## Supplementary Information

### Benchmarking TERS and TEPL probes: towards a reference sample for quantification of near-field enhancement factors in gap and non-gap modes

James Kerfoot,<sup>\*a</sup> Elizabeth J. Legge,<sup>b</sup> Amy Collins,<sup>c</sup> Jasbinder Chauhan,<sup>c</sup> Kai Rossnagel,<sup>d,e</sup> Peter H. Beton,<sup>c</sup> Christopher J. Mellor,<sup>c</sup> Andrew J. Pollard,<sup>b</sup> Graham A. Rance<sup>\*a,f</sup> and Michael W. George<sup>\*f</sup>

<sup>a</sup> Nanoscale and Microscale Research Centre (nmRC), University of Nottingham, University Park, Nottingham, NG7 2RD, UK.

<sup>b</sup> National Physical Laboratory (NPL), Hampton Road, Teddington, TW11 0LW, UK.

<sup>c</sup> School of Physics and Astronomy, University of Nottingham, University Park, Nottingham, NG7 2RD, UK.

<sup>d</sup> Institut für Experimentelle und Angewandte Physik, Christian-Albrechts-Universität zu Kiel, Olshausenstr. 40, 24098 Kiel, Germany.

<sup>e</sup> Ruprecht Haensel Laboratory, Deutsches Elektronen-Synchrotron DESY, Notkestr. 85, 22607 Hamburg, Germany.

<sup>f</sup> School of Chemistry, University of Nottingham, University Park, Nottingham, NG7 2RD, UK.

\* Corresponding author e-mail addresses: James Kerfoot ([james.kerfoot3@nottingham.ac.uk](mailto:james.kerfoot3@nottingham.ac.uk)), Graham A. Rance ([graham.rance@nottingham.ac.uk](mailto:graham.rance@nottingham.ac.uk)), Michael W. George ([michael.george@nottingham.ac.uk](mailto:michael.george@nottingham.ac.uk)).

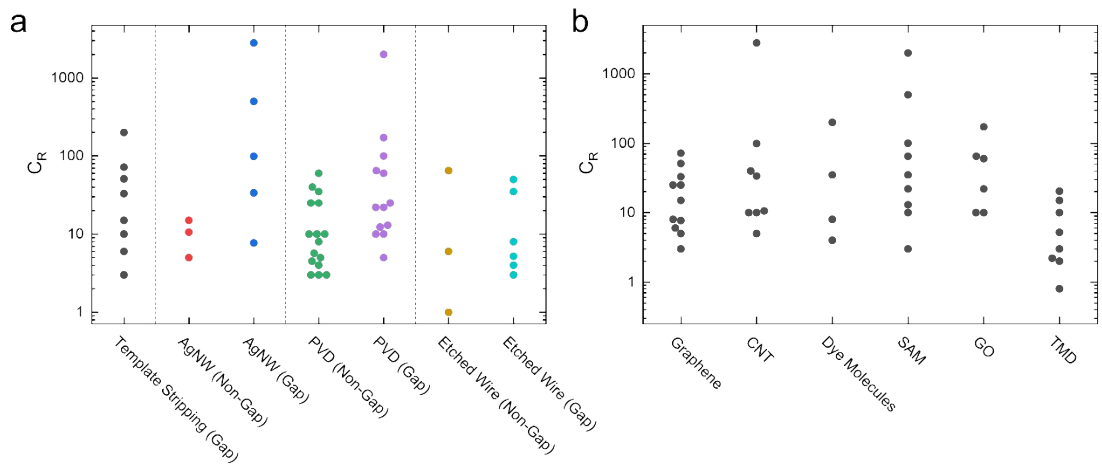


**Figure S1.** A plot of the reported Raman contrast factors ( $C_R$ ) calculated from a range of probe fabrication methods and substrate configurations (across multiple material classes) (a) and a range of materials, including graphene, carbon nanotubes (CNT), dye molecules, self-assembled monolayers (SAM), graphene oxide (GO) and transition metal dichalcogenides (TMD) (across multiple probe fabrication methods and substrate configurations) (b). Further details for each data point are given in Table S1.

**Table S1.** Details of the probe preparation, sample class, laser wavelength and reported  $C_R$  from literature studies, as shown in Figure S1. The following abbreviations are used throughout the table: single-walled carbon nanotube (SWNT), carbon nanotube (CNT), graphene oxide (GO), self-assembled monolayer (SAM), poly(3,4-ethylenedioxythiophene) (PEDOT), poly(vinyl alcohol) (PVA) and 4-nitrothiophenol (NTP).

Supplementary Information Reference and Method	Probe Apex Material	Sample	Substrate	Laser wavelength (nm)	$C_R$
Template Stripping (Non-Gap Mode)					
1	Au	Graphene	Glass	633	51
2	Au	Graphene	Glass	633	72
3	Au	Graphene	Glass	633	3
4	Au	Graphene	Glass	633	33
5	Au	SWNT	Glass	633	10
5	Au	Dye Molecules (Atto 647N)	Glass	785	200
6	Au	Graphene	Glass	633	15
6	Au	Graphene	Au on Glass	633	6
Ag Nanowires (Non-Gap Mode)					
7	Ag	SWNT	Si	633	10.6
8	Ag	1L-MoSe <sub>2</sub> and 1L-WSe <sub>2</sub>	SiO <sub>2</sub>	633	15
9	Ag	Graphene	SiO <sub>2</sub>	532	4.4
Ag Nanowires (Gap Mode)					
10	Ag	Graphene	Ag	532	7.7
11	Ag	Thiol (HS-C <sub>6</sub> H <sub>12</sub> -O-azobenzene)	Au	633	500
7	Ag	SWNT	Au	633	2800
7	Ag	SWNT	Au	633	33.7
12	Ag	SWNT	Au	633	99
Physical Vapour Deposition (Non-Gap Mode)					
13	Ag	Dye molecules (brilliant cresyl blue)	Glass	488	4
14	Ag	Graphene	Glass	488	25
15	Ag	CNT	Glass	488	5
16	Ag	PEDOT	PEDOT	532	3
17	Ag	Polystyrene	Polystyrene	532	3
17	Ag	CNT	Glass	532	10
18	Ag	Dye molecules (crystal violet)	Glass	532	35
19	Ag	MoS <sub>2</sub>	SiO <sub>2</sub>	532	3
20	Ag	Graphene	Glass	532	8
21	Ag	Zeolite	Resin	532	10
22	Ag	CNT	PVA on glass	532	40
14	Ag	Graphene	Glass	488	25
23	Ag	Lipid Bilayer	Glass	532	60

24	Ag	Solar Cell	Bulk	532	4.5
25	Ag	GO	Glass	532	10
26	Ag	Mouse Cell	Resin	532	5.7
Physical Vapour Deposition (Gap Mode)					
27	Ag	GO	Au	633	22
27	Ag	GO	Au	633	172
28	Ag	SAM (biphenyl thiol)	Au	532	10
17	Ag	SAM (biphenyl thiol)	Au	532	13
29	Au	CdSe	Au	638	25
30	Au	NTP	Ag	633	65
31	Au	NTP	Ag	633	100
32	Au	DNA	Au	633	12.3
33	Au	GO	Au	638	10
34	Au	GO	Au	638	60
35	Au	SAM (4-aminothiophenol )	Au	642	2000
36	Au	RNA	Au	660	5
Etched Wire (Non-Gap)					
37	Ag	Graphite	Graphite	532	6
25	Ag	GO	Glass	532	65
38	Au	Graphene	Glass	633	1
Etched Wire (Gap)					
39	Au	Dye molecules (brilliant cresyl blue)	Au	633	35
40	Au	SAM (4-nitrothiophenol)	Au	633	3
41	Au	Protein	Au	638	50
42	Ag	Dye molecules (Cu phthalocyanine)	Au	514	4
43	Au	Dye molecules (malachite green)	Au	633	8
44	Au	WS <sub>2</sub>	Au	633	5.2

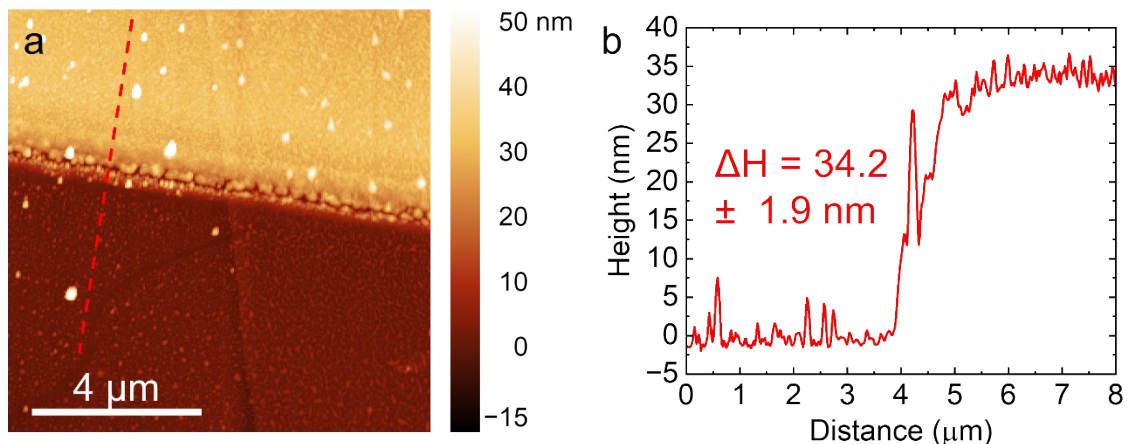


**Figure S2.** An AFM image of the reference sample discussed in Figures 1-3 of the main manuscript is shown (a), along with an extracted line profile – the location of which is indicated with a red dashed line in (a) – is plotted in (b).

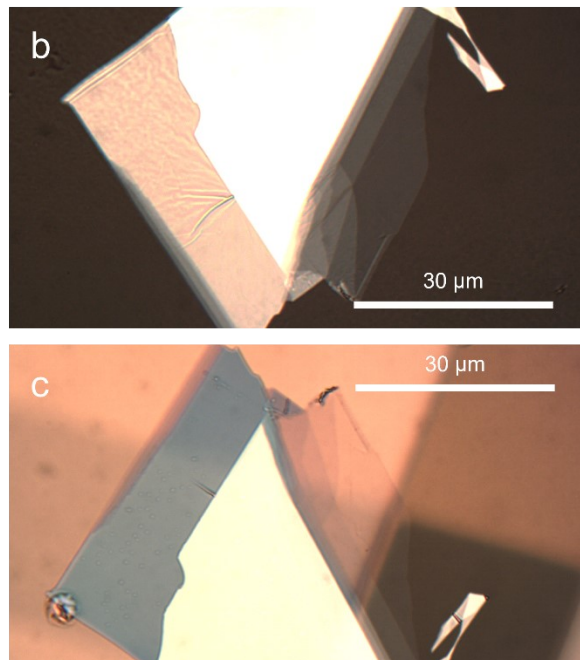
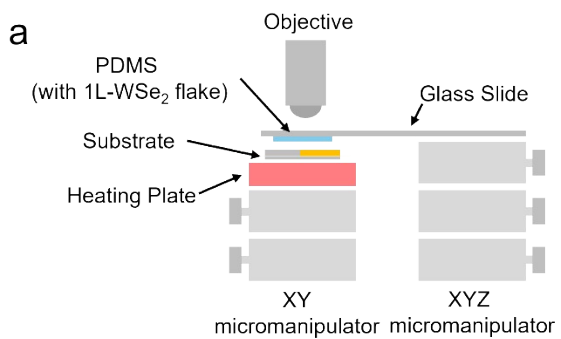


**Figure S3.** A schematic showing the operation of the transfer apparatus is shown (a) in addition to optical micrographs of a WSe<sub>2</sub> flake prepared by micromechanical cleavage with areas of monolayer and thicker regions before (b) and after (c) transfer from the PDMS stamp to an Au on glass substrate.

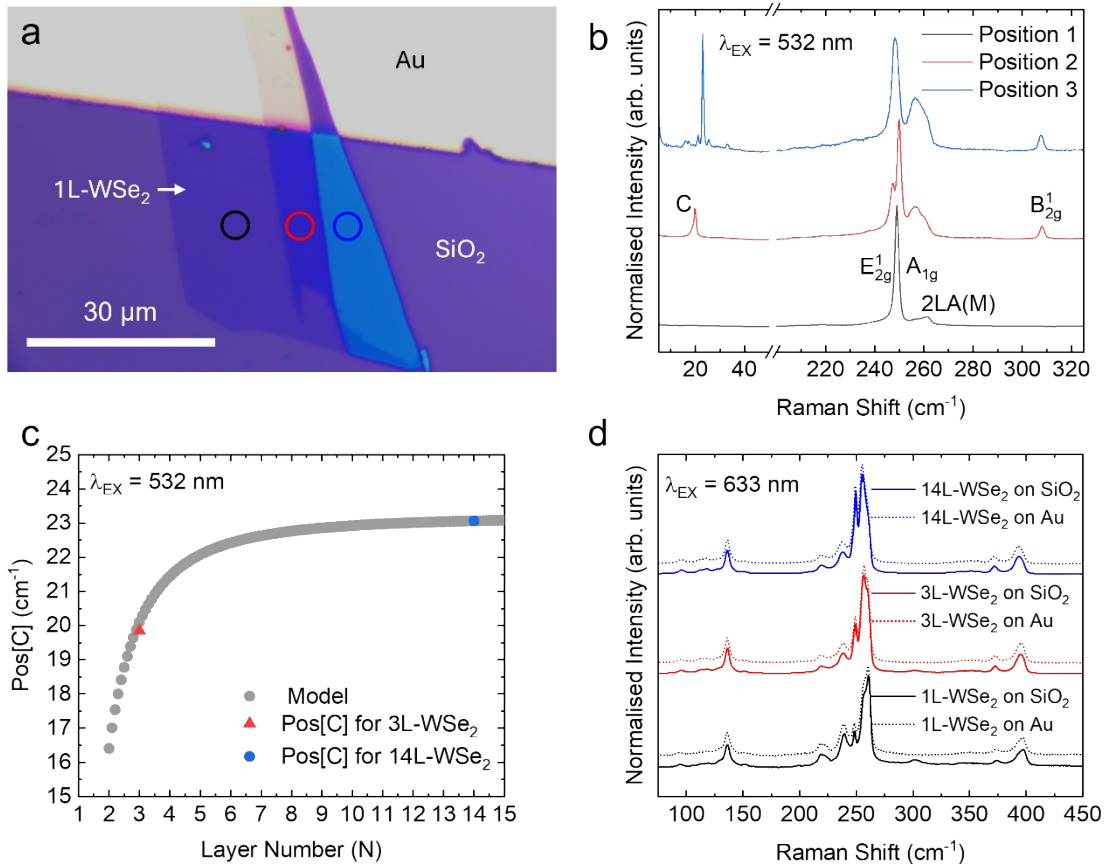


**Figure S4.** Far-field micro-Raman spectroscopy characterisation of the WSe<sub>2</sub> flake used for evaluation of probe performance in reflection mode TERS and TEPL, as discussed in Figures 1, 2 and 3 of the main manuscript. Single-point Raman spectra (532 nm excitation laser at 0.88 mW power) from locations corresponding to three different thicknesses of WSe<sub>2</sub> (denoted by coloured circles in the optical micrograph (a)) are shown (b), with the absence of the B<sub>2g</sub><sup>1</sup> mode inferring 1L-WSe<sub>2</sub> was present at the location of the black circle. The specific number of layers from multilayer areas was extracted using the position of the characteristic C mode correlated with the linear chain model (c),<sup>45</sup> with regions marked with red and blue circles corresponding to 3L- and 14L-WSe<sub>2</sub>, respectively. A comparison between the single-point Raman spectra (633 nm excitation laser at 0.77 mW power) for each layer thickness of WSe<sub>2</sub> on SiO<sub>2</sub> and Au is shown (d), indicating the far-field spectra are independent of the substrate. It is important to note that the spectra acquired with a 633 nm laser (d) show the same first order bands as the corresponding spectra acquired with a 532 nm laser (b), but additional harmonics and overtones are observed due to resonance effects.<sup>46</sup> Thus, the Raman spectra acquired with a 633 nm laser shown here can be classified as resonance Raman spectra, in the same way that the TERS spectra shown in Figure 1 (also with a 633 nm laser) can be described as tip-enhanced resonance Raman scattering (TERRS) spectra; however, for the sake of simplicity, we have not made this distinction elsewhere.

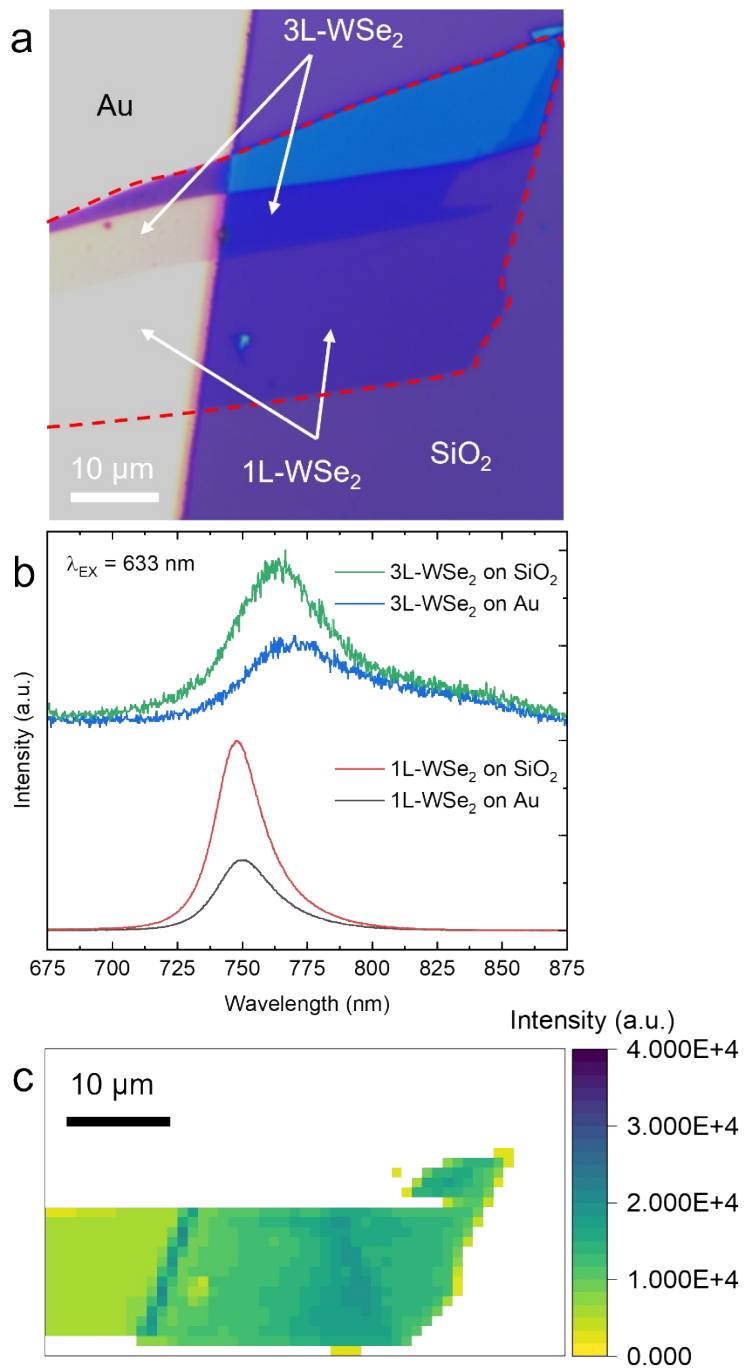


**Figure S5.** An optical micrograph of the 1L-WSe<sub>2</sub> sample used for probe performance evaluation in reflection mode TERS and TEPL discussed in Figures 1, 2 and 3 of the main manuscript is shown (a) in addition to single-point photoluminescence spectra recorded from 1L- and 3L-WSe<sub>2</sub> regions on SiO<sub>2</sub> and Au (b) confirming the 1L- assignation determined from micro-Raman measurements (Figure S4), with 1L-WSe<sub>2</sub> showing strong and relatively uniform photoluminescence from the monolayer area of the flake. The spectra have been normalised such that the spectra obtained on Au are of equal intensity. Hyperspectral photoluminescence imaging was performed to show the spatial distribution of the total integrated signal intensity from the 1L-WSe<sub>2</sub> flake (c). Note, the 3L- and 14L-WSe<sub>2</sub> regions and flake-free areas were excluded from (c) by intensity thresholding.

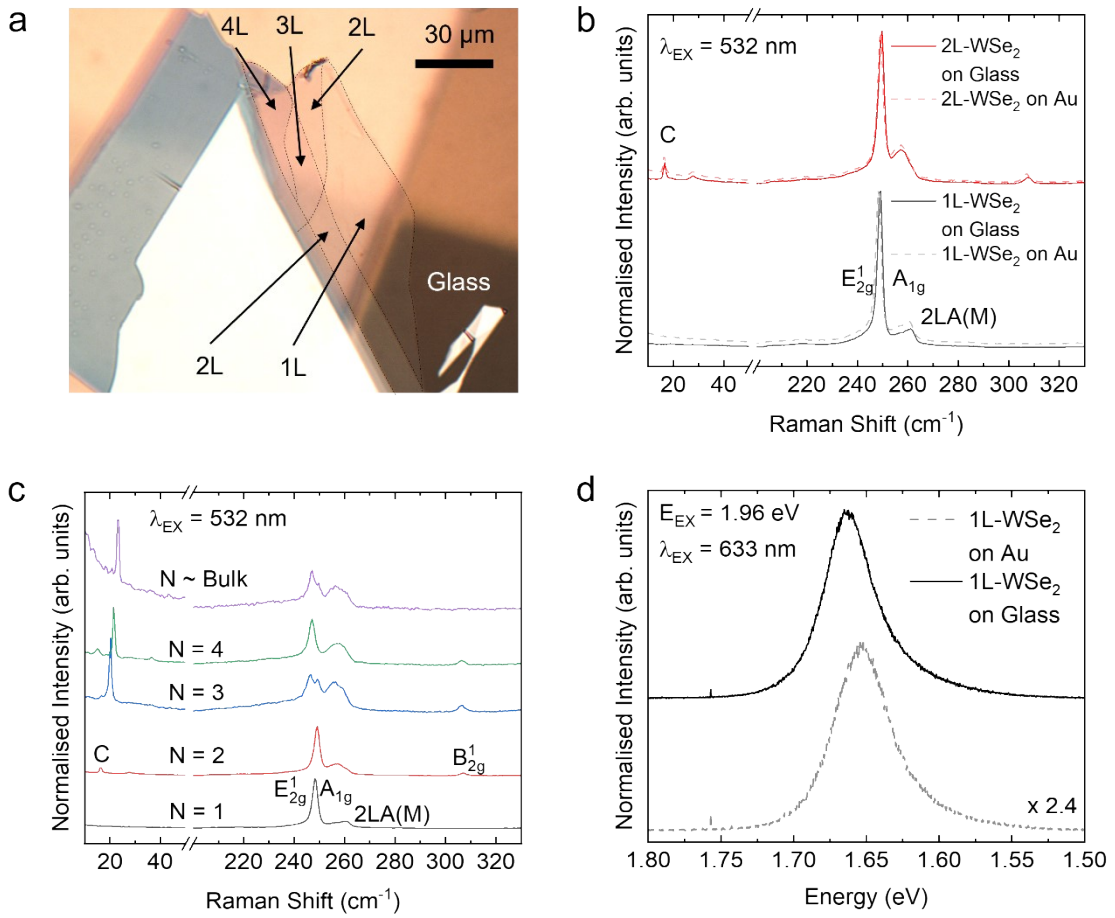


**Figure S6.** Far-field micro-Raman and photoluminescence spectroscopy characterisation of the WSe<sub>2</sub> flake (a) used for evaluation of probe performance in transmission mode TERS discussed in Figure 4 of the main manuscript. Single-point Raman spectra (532 nm laser) obtained from different locations are indicative of the 1L- and 2L- nature of WSe<sub>2</sub> on glass and Au (b). The layer thickness of the different areas of the sample annotated in (a) were verified using both ultra-low frequency Raman spectroscopy (c) and photoluminescence spectroscopy (d) characterisation of the monolayer region of the sample on and off the Au film.

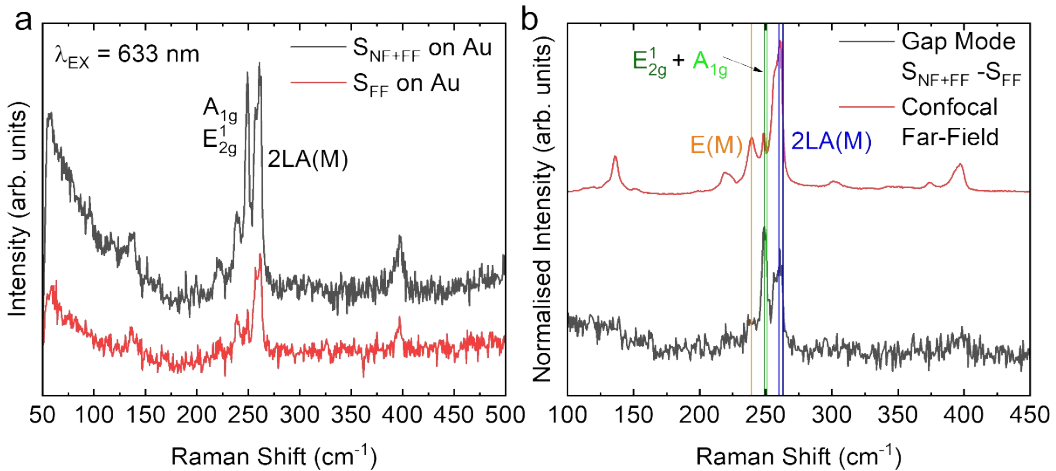


**Figure S7.** Higher spectral resolution spectra recorded with the probe in contact ( $S_{NF+FF}$ ) and retracted ( $S_{FF}$ ) from 1L-WSe<sub>2</sub> on Au (a) and a comparison of the far-field subtracted data with the confocal Raman spectrum with literature<sup>46-49</sup> Raman mode assignments for 1L-WSe<sub>2</sub> (b). Spectra were acquired with a 600 l mm<sup>-1</sup> diffraction grating and a probe of lower  $C_R$  under the same experimental conditions used for Figure 1 of the main manuscript. Here, signal contribution from the far-field was significant; however, the amplification of the combined  $A_{1g}$  and  $E_{2g}^1$  modes, relative to the  $2\text{LA}(M)$  mode, in the near-field plus far-field spectrum is clear, thus providing compelling evidence for the preferential enhancement of the in-plane ( $A_{1g}$ ) mode in the near-field spectrum in gap mode. It is important to note that as the  $A_{1g}$  and  $E_{2g}^1$  modes are degenerate their respective contributions cannot be deconvoluted. Thus, low spectral resolution data, including that collected using a 150 l mm<sup>-1</sup> diffraction grating, as shown in Figure 1 of the main manuscript, is sufficient to enable meaningful quantification of  $C_R$ , with the additional advantage that low resolution set-ups provide a broad spectral window sufficient to examine both TERS and TEPL simultaneously. TERS measurements were performed with a 633 nm excitation source at a power of 0.15 mW. If we assume the in-plane  $2\text{LA}(M)$  and  $E_{2g}^1$  modes are enhanced to the same extent in gap mode, by extracting peak ratios ( $2\text{LA}(M):E_{2g}^1+A_{1g}$ ) and applying simultaneous equations we can tentatively comment on the preferential enhancement of the out-of-plane  $A_{1g}$  mode. From this analysis, we determine in-plane and out-of-plane  $C_R$  values of ~2 and ~12, respectively, corresponding to a ~6 fold increase which can be ascribed to an enhancement of the out-of-plane electric fields arising from coupling to the plasmonic substrate in gap mode.

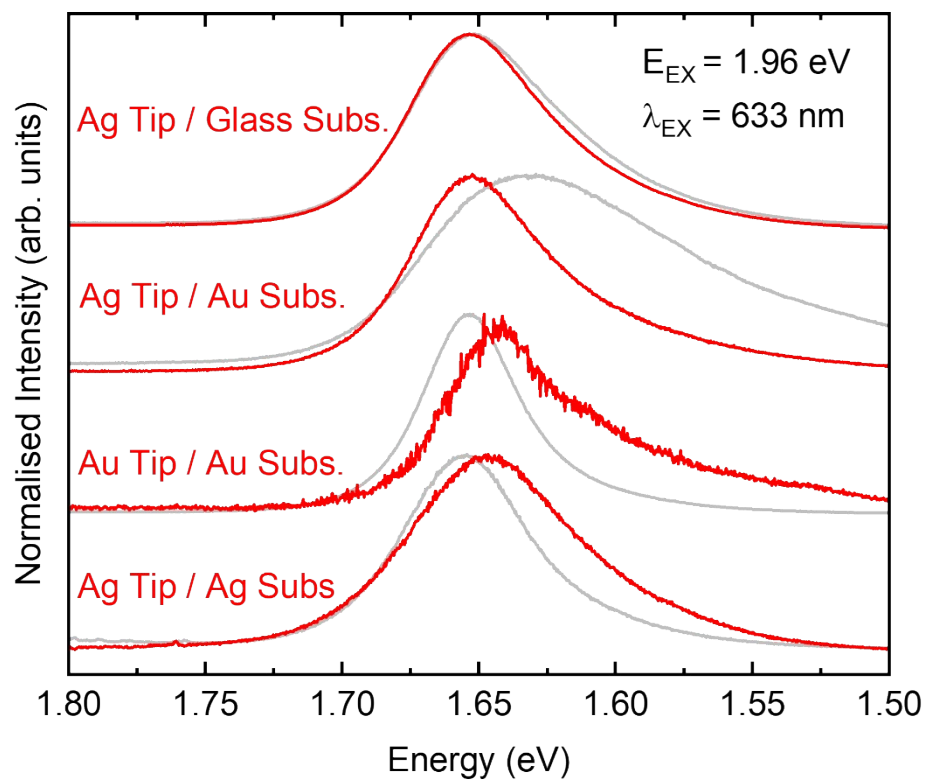


**Figure S8.** Normalised  $S_{NF+FF}$  -  $S_{FF}$  (red) and  $S_{FF}$  (grey) photoluminescence spectra of several combinations of probe and substrate materials (labelled inset) acquired with a 633 nm excitation source at a power of 0.15 mW.

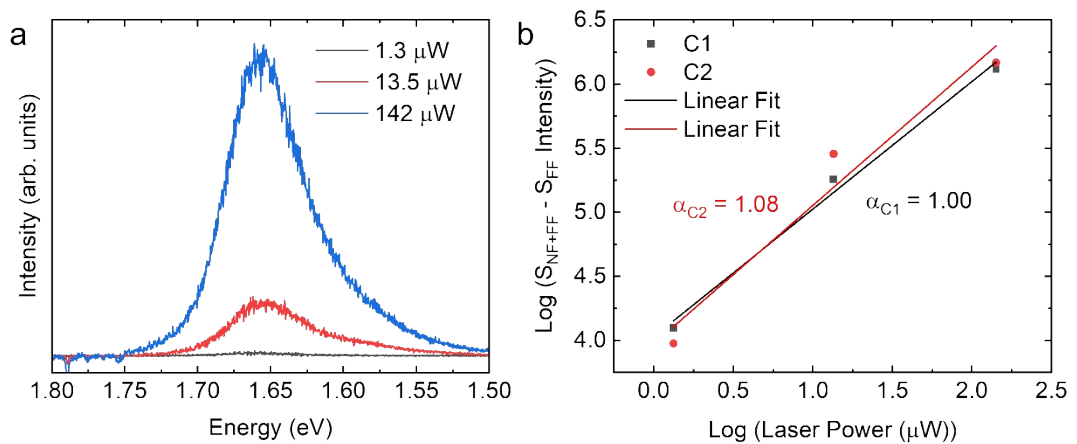


**Figure S9.** The power dependence of the far-field-subtracted TEPL spectra ( $S_{NF+FF} - S_{FF}$ ) recorded from 1L-WSe<sub>2</sub> on Au in reflection mode is shown (a) in addition to a log plot of the intensities extracted from a two-component Lorentzian fit (b). Component 1 is centred at ~1.66 eV and component 2 is centred at ~1.64 eV.

**Table S2.** A proposed set of desirable characteristics for a TERS and TEPL reference sample. The specifications noted here are not intended to be exhaustive or definitive but are designed to tentatively guide further development in this area. A critical appraisal of how well our 1L-WSe<sub>2</sub> reference sample meets these criteria is presented, along with commentary on the potential modifications to this reference sample or alternative reference samples previously described in the literature (specifically, carbon nanotubes (CNT)<sup>28, 50</sup> or self-assembled monolayers (SAM) of organic molecules<sup>51</sup> on Au) that would enable these to be fully met is discussed. Information on general reference sample requirements can be found in ISO 17034:2016(en) and ISO 33403:2024.

Criterion	Descriptor	Criterion met?	Comments	Alternatives
<b>1</b>	<b>General requirements</b>			
1.1	Relevance to a real-life sample	Yes	WSe <sub>2</sub> is a nanomaterial of interest in the TERS/TEPL community.	CNT, SAM, MoS <sub>2</sub> .
1.2	Quantification of probe sensitivity or enhancement	Yes	Tested at UoN (Figures 1-3) and NPL (Figure 4).	SAM.
1.3	Quantification of spatial resolution	No	In principle, nanoscale patterns in the 1L-WSe <sub>2</sub> could be engineered using lithographic techniques to enable quantification of limiting spatial resolution, as has been shown previously for SAM on Au. <sup>51</sup>	SAM would require lithographic patterning. CNT have dimensions that are appropriate, though variations in diameter would need to be accounted for.
1.4	Suitable for reflection mode	Yes	Tested at UoN (Figures 1-3).	CNT, SAM on Au.
1.5	Suitable for transmission mode	Yes	Tested at NPL (Figure 4). A transparent substrate and thin Au layer (~10 nm) were essential.	CNT, SAM on a thin Au layer.
1.6	Suitable for multiple wavelengths of excitation laser	Yes	Excitation wavelengths of 633 nm and 532 nm were tested at UoN (TERS and TEPL) and NPL (TERS), respectively.	
1.7	Suitable for gap mode	Yes	Tested at UoN (Figures 1-3) and NPL (Figure 4).	CNT, SAM.
1.8	Suitable for non-gap mode	Yes	Tested at UoN (Figures 1-3) and NPL (Figure 4).	CNT.
1.9	TERS signal	Yes	Tested at UoN (Figure 1) and NPL (Figure 4).	CNT, SAM.
1.10	TEPL signal	Yes	Tested at UoN (Figures 2 and 3).	SAM with visible fluorophores might enable this.
<b>2</b>	<b>Sample features</b>			
2.1	Area of interest identifiable with optical microscopy, or covering the whole sample	Yes	Demonstrated in Figure 1.	
2.2	Uniform chemical and physical composition	Partially	Small changes in surface roughness, but uniform concentration (thickness) and at least initially	

			chemically uniform.	
2.3	Stable under ambient conditions	Partially	WSe <sub>2</sub> is relatively stable under ambient conditions, however, gradual oxidation can occur, therefore storage under vacuum or inert atmosphere is preferable. <sup>52</sup>	
2.4	Stable when exposed to lasers	Partially	We observed no spectral changes that would be diagnostic of damage and/or photobleaching up to a laser power of 0.77 mW. However, damage would be expected (as with most samples) at high laser power.	CNT, SAM.
2.5	Mechanically robust when the probe is in contact with the sample	Yes	The sample discussed in Figure 2 was measured with multiple probes and found to be mechanically robust under all conditions applied.	CNT.
2.6	Robust sample for shipping and handling at multiple laboratories	Partially	The substrate in Figure 4 is susceptible to mechanical breakages, however it was successfully shipped between laboratories using appropriate packaging.	CNT, SAM.
<b>3</b>	<b>Spectral features</b>			
3.1	At least one peak between 200 cm <sup>-1</sup> and 2000 cm <sup>-1</sup>	Yes	Several measurable Raman peaks with the range ~240-265 cm <sup>-1</sup> .	CNT and SAM both exhibit Raman modes above 200 cm <sup>-1</sup> .
3.2	At least one peak between 1.5 eV and 1.8 eV	Yes	Possesses PL emission at ~1.65 eV.	
3.3	Distinct in-plane and out-of-plane modes	Yes	The out-of-plane A <sub>1g</sub> and in-plane E <sup>1</sup> <sub>2g</sub> modes of 1L-WSe <sub>2</sub> are degenerate, though the PL contains contributions from exitonic species with in-plane and out-of-plane transition dipole moments.	Related transition metal dichalcogenides exhibit non-degenerate A <sub>1g</sub> and E <sup>1</sup> <sub>2g</sub> modes, but their spectra can be complicated by overlapping Raman and PL emissions (depending on excitation laser wavelength).
3.4	Easily isolated or identifiable peak	Yes		
<b>4</b>	<b>Sample preparation</b>			
4.1	Trivial to prepare	Yes		
4.2	Safe to handle	After preparation	WSe <sub>2</sub> does present H301+H331 and H373 hazard codes, but standard health and safety provisions enable the safe handling of these materials. Once prepared and adhered to a non-hazardous substrate, the sample hazards are significantly	The preparation of SAM, particularly those based upon highly toxic thiophenol derivatives, requires specialist handling. MoS <sub>2</sub>

			reduced.	has no known hazards.
4.3	Easy route to commercialisation	Yes	A simple cost analysis reveals that ten samples could be manufactured for as little as ~\$200 each. As such, we anticipate future potential for commercialisation.	CNT on Au and SAM on Au samples are commercially available.

## Supplementary Information References

1. B. S. Oliveira, B. S. Archanjo, R. Valaski, C. A. Achete, L. G. Cançado, A. Jorio and T. L. Vasconcelos, *J. Chem. Phys.*, 2020, **153**, 114201.
2. T. L. Vasconcelos, B. S. Archanjo, B. S. Oliveira, W. F. Silva, R. S. Alencar, C. Rabelo, C. A. Achete, A. Jorio and L. G. Cançado, *IEEE J. Sel. Top. Quantum Electron.*, 2021, **27**, 1-11.
3. R. Beams, L. G. Cançado, S.-H. Oh, A. Jorio and L. Novotny, *Phys. Rev. Lett.*, 2014, **113**, 186101.
4. T. L. Vasconcelos, B. S. Archanjo, B. S. Oliveira, R. Valaski, R. C. Cordeiro, H. G. Medeiros, C. Rabelo, A. Ribeiro, P. Ercius, C. A. Achete, A. Jorio and L. G. Cançado, *Adv. Opt. Mater.*, 2018, **6**, 1800528.
5. T. W. Johnson, Z. J. Lapin, R. Beams, N. C. Lindquist, S. G. Rodrigo, L. Novotny and S.-H. Oh, *ACS Nano*, 2012, **6**, 9168-9174.
6. H. Miranda, C. Rabelo, L. G. Cançado, T. L. Vasconcelos, B. S. Oliveira, F. Schulz, H. Lange, S. Reich, P. Kusch and A. Jorio, *Phys. Rev. Res.*, 2020, **2**, 023408.
7. H. Wen, J. Li, Q. Zhang, T. Inose, W. Peeters, B. Fortuni, H. Asakawa, A. Masuhara, K. Hirai, S. Toyouchi, Y. Fujita and H. Uji-i, *Nano Lett.*, 2023, **23**, 1615-1621.
8. W. Peeters, S. Toyouchi, Y. Fujita, M. Wolf, B. Fortuni, E. Fron, T. Inose, J. Hofkens, T. Endo, Y. Miyata and H. Uji-i, *ACS Omega*, 2023, **8**, 38386-38393.
9. P. Walke, S. Toyouchi, M. Wolf, W. Peeters, S. R. Prabhu, T. Inose, S. De Feyter, Y. Fujita and H. Uji-i, *J. Phys. Chem. Lett.*, 2018, **9**, 7117-7122.
10. Q. Liu, S. Kim, X. Ma, N. Yu, Y. Zhu, S. Deng, R. Yan, H. Zhao and M. Liu, *Nanoscale*, 2019, **11**, 7790-7797.
11. P. Walke, Y. Fujita, W. Peeters, S. Toyouchi, W. Frederickx, S. De Feyter and H. Uji-i, *Nanoscale*, 2018, **10**, 7556-7565.
12. H. Wen, T. Inose, K. Hirai, T. Akashi, S. Sugioka, J. Li, W. Peeters, E. Fron, B. Fortuni, Y. Nakata, S. Rocha, S. Toyouchi, Y. Fujita and H. Uji-i, *Nanoscale*, 2022, **14**, 5439-5446.
13. B.-S. Yeo, W. Zhang, C. Vannier and R. Zenobi, *Appl. Spectrosc.*, 2006, **60**, 1142-1147.
14. A. Taguchi, J. Yu, P. Verma and S. Kawata, *Nanoscale*, 2015, **7**, 17424-17433.
15. T. Mino, Y. Saito and P. Verma, *ACS Nano*, 2014, **8**, 10187-10195.
16. N. Kumar, C. S. Wondergem, A. J. Wain and B. M. Weckhuysen, *J. Phys. Chem. Lett.*, 2019, **10**, 1669-1675.
17. N. Kumar, W. Su, M. Veselý, B. M. Weckhuysen, A. J. Pollard and A. J. Wain, *Nanoscale*, 2018, **10**, 1815-1824.
18. A. Capaccio, A. Sasso, O. Tarallo and G. Rusciano, *Nanoscale*, 2020, **12**, 24376-24384.
19. T. Verhagen, A. Rodriguez, M. Vondráček, J. Honolka, S. Funke, M. Zlámalová, L. Kavan, M. Kalbac, J. Vejpravova and O. Frank, *ACS Appl. Nano Mater.*, 2020, **3**, 6563-6573.
20. E. J. Legge, K. R. Paton, M. Wywias, G. McMahon, R. Pemberton, N. Kumar, A. P. Aranga Raju, C. P. Dawson, A. J. Strudwick, J. W. Bradley, V. Stolojan, S. R. P. Silva, S. A. Hodge, B. Brennan and A. J. Pollard, *ACS Appl. Mater. Interfaces*, 2020, **12**, 13481-13493.
21. N. Kumar, S. Kalirai, A. J. Wain and B. M. Weckhuysen, *ChemCatChem*, 2019, **11**, 417-423.
22. N. Hayazawa, T.-a. Yano and S. Kawata, *J. Raman Spectrosc.*, 2012, **43**, 1177-1182.
23. D. Mrđenović, Z.-X. Tang, Y. Pandey, W. Su, Y. Zhang, N. Kumar and R. Zenobi, *Nano Lett.*, 2023, **23**, 3939-3946.
24. S. Bienz, G. Spaggiari, D. Calestani, G. Trevisi, D. Bersani, R. Zenobi and N. Kumar, *ACS Appl. Mater. Interfaces*, 2024, **16**, 14704-14711.
25. L. Ramanauskaitė, H. Xu, E. Griskonis, D. Batiuskaite and V. Snitka, *Plasmonics*, 2018, **13**, 1907-1919.
26. N. Kumar, M. M. Drozdz, H. Jiang, D. M. Santos and D. J. Vaux, *Chem. Commun.*, 2017, **53**, 2451-2454.
27. V. Kesava Rao, K. K. H. De Silva and M. Yoshimura, *Appl. Surf. Sci.*, 2022, **577**, 151937.
28. N. Kumar, B. M. Weckhuysen, A. J. Wain and A. J. Pollard, *Nat. Protoc.*, 2019, **14**, 1169-1193.

29. I. A. Milekhin, M. Rahaman, K. V. Anikin, E. E. Rodyakina, T. A. Duda, B. M. Saidzhonov, R. B. Vasiliev, V. M. Dzhagan, A. G. Milekhin, A. V. Latyshev and D. R. T. Zahn, *Nanoscale Adv.*, 2020, **2**, 5441-5449.
30. C.-F. Wang, B. T. O'Callahan, D. Kurouski, A. Krayev, Z. D. Schultz and P. Z. El-Khoury, *J. Phys. Chem. Lett.*, 2020, **11**, 5890-5895.
31. C.-F. Wang, B. T. O'Callahan, D. Kurouski, A. Krayev and P. Z. El-Khoury, *J. Phys. Chem. Lett.*, 2020, **11**, 3809-3814.
32. X. You, C. B. Casper, E. E. Lentz, D. A. Erie and J. M. Atkin, *ChemPhysChem*, 2020, **21**, 188-193.
33. W. Su, N. Kumar, A. Krayev and M. Chaigneau, *Nat. Commun.*, 2018, **9**, 2891.
34. A. Bhattacharai, A. Krayev, A. Temiryazev, D. Evplov, K. T. Crampton, W. P. Hess and P. Z. El-Khoury, *Nano Lett.*, 2018, **18**, 4029-4033.
35. K. Uetsuki, P. Verma, P. Nordlander and S. Kawata, *Nanoscale*, 2012, **4**, 5931-5935.
36. Z. He, W. Qiu, M. E. Kizer, J. Wang, W. Chen, A. V. Sokolov, X. Wang, J. Hu and M. O. Scully, *ACS Photonics*, 2021, **8**, 424-430.
37. J. S. Lloyd, A. Williams, R. H. Rickman, A. McCowen and P. R. Dunstan, *Appl. Phys. Lett.*, 2011, **99**, 143108.
38. T. L. Vasconcelos, B. S. Archanjo, B. Fragneaud, B. S. Oliveira, J. Riikonen, C. Li, D. S. Ribeiro, C. Rabelo, W. N. Rodrigues, A. Jorio, C. A. Achete and L. G. Cançado, *ACS Nano*, 2015, **9**, 6297-6304.
39. H. Lee, J. Y. Jeong, H. Kim, W. Park and S. Choi, *Curr. Appl. Phys.*, 2021, **32**, 86-90.
40. C. Awada, C. Dab, J. Zhang and A. Ruediger, *J. Raman Spectrosc.*, 2020, **51**, 1270-1277.
41. C. D'Andrea, A. Foti, M. Cottat, M. Banchelli, C. Capitini, F. Barreca, C. Canale, M. de Angelis, A. Relini, O. M. Maragò, R. Pini, F. Chiti, P. G. Gucciardi and P. Matteini, *Small*, 2018, **14**, 1800890.
42. R. D. Rodriguez, E. Sheremet, S. Müller, O. D. Gordan, A. Villabona, S. Schulze, M. Hietschold and D. R. T. Zahn, *Rev. Sci. Instrum.*, 2012, **83**, 123708.
43. S. Berweger, J. M. Atkin, R. L. Olmon and M. B. Raschke, *J. Phys. Chem. Lett.*, 2010, **1**, 3427-3432.
44. C. Lee, S. T. Kim, B. G. Jeong, S. J. Yun, Y. J. Song, Y. H. Lee, D. J. Park and M. S. Jeong, *Sci. Rep.*, 2017, **7**, 40810.
45. G. Pizzi, S. Milana, A. C. Ferrari, N. Marzari and M. Gibertini, *ACS Nano*, 2021, **15**, 12509-12534.
46. E. del Corro, H. Terrones, A. Elias, C. Fantini, S. Feng, M. A. Nguyen, T. E. Mallouk, M. Terrones and M. A. Pimenta, *ACS Nano*, 2014, **8**, 9629-9635.
47. E. del Corro, A. Botello-Méndez, Y. Gillet, A. L. Elias, H. Terrones, S. Feng, C. Fantini, D. Rhodes, N. Pradhan, L. Balicas, X. Gonze, J. C. Charlier, M. Terrones and M. A. Pimenta, *Nano Lett.*, 2016, **16**, 2363-2368.
48. W. Zhao, Z. Ghorannevis, K. K. Amara, J. R. Pang, M. Toh, X. Zhang, C. Kloc, P. H. Tan and G. Eda, *Nanoscale*, 2013, **5**, 9677-9683.
49. H. Terrones, E. D. Corro, S. Feng, J. M. Poumirol, D. Rhodes, D. Smirnov, N. R. Pradhan, Z. Lin, M. A. T. Nguyen, A. L. Elías, T. E. Mallouk, L. Balicas, M. A. Pimenta and M. Terrones, *Sci. Rep.*, 2014, **4**, 4215.
50. C. Chen, N. Hayazawa and S. Kawata, *Nat. Commun.*, 2014, **5**, 3312.
51. A. Sacco, D. Imbraguglio, Andrea M. Giovannozzi, C. Portesi and A. M. Rossi, *RSC Adv.*, 2018, **8**, 27863-27869.
52. L. Gammelgaard, P. R. Whelan, T. J. Booth and P. Bøggild, *Nanoscale*, 2021, **13**, 19238-19246.